# Three-dimensional radiobiological dosimetry of kidneys for treatment planning in peptide receptor radionuclide therapy

Sébastien Baechler[a)]
*Institute of Radiation Physics, Lausanne University Hospital, 1007 Lausanne, Switzerland*

Robert F. Hobbs
*The Russell H. Morgan Department of Radiology and Radiological Sciences, Johns Hopkins University, School of Medicine, Baltimore, Maryland 21231*

Ariane Boubaker and Franz Buchegger
*Department of Nuclear Medicine, Lausanne University Hospital, 1011 Lausanne, Switzerland*

Bin He, Eric C. Frey, and George Sgouros
*The Russell H. Morgan Department of Radiology and Radiological Sciences, Johns Hopkins University, School of Medicine, Baltimore, Maryland 21231*

(Received 26 April 2012; revised 29 July 2012; accepted for publication 28 August 2012; published 21 September 2012)

**Purpose:** Peptide receptor radionuclide therapy (PRRT) delivers high absorbed doses to kidneys and may lead to permanent nephropathy. Reliable dosimetry of kidneys is thus critical for safe and effective PRRT. The aim of this work was to assess the feasibility of planning PRRT based on 3D radiobiological dosimetry (3D-RD) in order to optimize both the amount of activity to administer and the fractionation scheme, while limiting the absorbed dose and the biological effective dose (BED) to the renal cortex.

**Methods:** Planar and SPECT data were available for a patient examined with $^{111}$In-DTPA-octreotide at 0.5 (planar only), 4, 24, and 48 h post-injection. Absorbed dose and BED distributions were calculated for common therapeutic radionuclides, i.e., $^{111}$In, $^{90}$Y and $^{177}$Lu, using the 3D-RD methodology. Dose-volume histograms were computed and mean absorbed doses to kidneys, renal cortices, and medullae were compared with results obtained using the MIRD schema (S-values) with the multiregion kidney dosimetry model. Two different treatment planning approaches based on (1) the fixed absorbed dose to the cortex and (2) the fixed BED to the cortex were then considered to optimize the activity to administer by varying the number of fractions.

**Results:** Mean absorbed doses calculated with 3D-RD were in good agreement with those obtained with S-value-based SPECT dosimetry for $^{90}$Y and $^{177}$Lu. Nevertheless, for $^{111}$In, differences of 14% and 22% were found for the whole kidneys and the cortex, respectively. Moreover, the authors found that planar-based dosimetry systematically underestimates the absorbed dose in comparison with SPECT-based methods, up to 32%. Regarding the 3D-RD-based treatment planning using a fixed BED constraint to the renal cortex, the optimal number of fractions was found to be 3 or 4, depending on the radionuclide administered and the value of the fixed BED. Cumulative activities obtained using the proposed simulated treatment planning are compatible with real activities administered to patients in PRRT.

**Conclusions:** The 3D-RD treatment planning approach based on the fixed BED was found to be the method of choice for clinical implementation in PRRT by providing realistic activity to administer and number of cycles. While dividing the activity in several cycles is important to reduce renal toxicity, the clinical outcome of fractionated PRRT should be investigated in the future.  [http://dx.doi.org/10.1118/1.4752213]

Key words: kidney dosimetry, peptide receptor radionuclide therapy, biological effective dose

## I. INTRODUCTION

Peptide receptor radionuclide therapy (PRRT) with radiolabeled somatostatin analogues is a promising treatment for patients with inoperable or metastasized neuroendocrine tumors (NETs).[1] Briefly, the principle of PRRT is based on the affinity of the radiolabeled peptide for specific tumor cell membrane receptors and the internalization of the receptor-peptide complex to increase the retention of the radionuclide inside tumor cells. Successful peptides for this purpose are somatostatin analogs that bind to somatostatin receptors overexpressed in NETs. Originally, somatostatin-based PRRT was performed with high dosages of $^{111}$In-DTPA-octreotide,[2] which was first designed for imaging purposes and is still routinely used for diagnosis and staging of NETs. Subsequently, DOTATOC and DOTATATE were developed as they showed higher binding affinity to most NETs[3] and were stably labeled with $^{90}$Y or $^{177}$Lu, which are potentially more effective

than $^{111}$In for treatment. Results from preclinical and clinical studies using either $^{90}$Y-DOTATOC or $^{177}$Lu-DOTATATE are encouraging in terms of observed tumor regressions and stabilization.[4] Only minor tumor responses were observed with $^{111}$In-DTPA-octreotide, probably due to the short tissue penetration of Auger electrons that are mainly emitted from tracer localized in cytoplasm and may not reach the cell nucleus. Clinical studies are ongoing to evaluate and compare the relative efficacies of those peptides labeled with either $^{90}$Y or $^{177}$Lu.[5]

While leading to tumor regression or stability for a majority of patients, PRRT using somatostatin analogs labeled with $^{90}$Y or $^{177}$Lu is potentially toxic to nontarget organs, particularly the kidneys. Indeed, large amounts of radiolabeled peptides are retained in the renal cortex and cause high radiation doses that may result in permanent loss of nephron mass and chronic renal failure.[6] As a result, high absorbed doses to the kidneys limit the activity that may be required to achieve clinically useful absorbed doses to tumors. Because of long-term renal toxicity, the high amounts of activity used in animals are not tolerable for patients and could explain why complete remissions are rarely obtained in clinical studies in contrast to animal studies.[7] One way to increase the amount of activity to administer is to reduce the renal uptake and thus the radiation dose to kidneys. Therefore, in clinical practice, PRRT is always being administered with renal-protective agents. Another way is to spare renal tissues by fractioning the cumulative administered activity into several cycles in order to allow repair of sublethal damage between cycles. Reliable dosimetric approaches including fractionation are thus critical for individualized treatment planning in order to maximize the cumulative activity to administer, and thus potentially the therapeutic efficacy, while keeping a safe cumulative dose of radiation to the kidneys.[4,8]

Kidney dosimetry is traditionally assessed using the medical internal radiation dose (MIRD) methodology,[9] which assumes a uniform activity distribution within the kidneys. Since peptides are mainly deposited in the proximal tubules in the renal cortex, which is associated with a greater radiobiological sensitivity, the localization of the absorbed dose may increase the risk of renal toxicity. MIRD Pamphlet No. 19 (MIRD19) addressed this issue by dividing the kidney into cortex, medulla, and renal pelvis compartments[10] and provided an estimate of the average dose to the cortex. Using the MIRD19 models, Barone *et al.*[11] demonstrated that the biological effective dose (BED) was a more appropriate quantity than absorbed dose to predict the dose-response relationship for renal toxicity in PRRT. The BED relates absorbed dose and dose rate to radiosensitivity and repair using the linear-quadratic model.[12,13] More precisely, the BED gives the absorbed dose that should be delivered to a tissue for a certain biological effect at an infinitesimally small dose rate and is useful to compare treatments with different dose rates and fractionation schemes. The use of the BED concept for renal dosimetry was expanded upon in MIRD Pamphlet No. 20.[14]

The aim of this work was to propose a reliable treatment planning methodology for PRRT based on 3D radiobiological dosimetry (3D-RD), which would translate the current knowledge of renal toxicity and state-of-the-art 3D dosimetry into clinically applicable optimized treatment planning. The preexisting 3D-RD methodology combines 3D imaging-based dosimetry with radiobiological modeling,[15,16] and accounts for both nonuniformity in kidneys and dose-rate differences by providing a BED value for the volumes of interest (VOIs). In this work, we expand and assess the application of this methodology to PRRT in order to enable the calculation of the optimal amount of activity to administer and the optimal fractionation scheme while limiting the absorbed dose or the BED to the renal cortex.

## II. MATERIALS AND METHODS

### II.A. Patient data

A 39-year-old male patient with clinically suspected NETs was examined at the Lausanne University Hospital in the context of a prospective clinical study. He was injected with 185 MBq of $^{111}$In-DTPA-octreotide (Octreoscan, Mallinckrodt Medical, Petten, The Netherlands). Planar whole-body images were acquired at 0.5, 4, 24, and 48 h post-injection (p.i.) on a dual-head gamma-camera (Biad; Trionix Research Laboratory, Inc., Twinsburg, OH) in a 256 × 1024 matrix, using a medium-energy collimator, and 15% energy windows centered at 171 and 245 keV. In addition, SPECT acquisitions of the abdominal region were performed at 4, 24, and 48 h p.i. with a three-head gamma-camera (Triad; Trionix Research Laboratory, Inc., Twinsburg, OH) in a 128 × 128 matrix (4.48 × 4.48 mm$^2$) with 120 projections (40 s/projection), using a medium-energy collimator and 20% energy windows centered at 171 and 245 keV.

### II.B. Image-based activity quantification

For planar imaging, the conjugate view method was used to calculate mean activity uptake in the whole body, liver, and spleen.[17] Correction for attenuation was based on a whole-body average-attenuation factor obtained from the data acquired before voiding, i.e., at 0.5 h p.i. For the kidneys, the single-view effective point source method, including background subtraction, was used to determine the mean activity. This method has been described in detail elsewhere.[18]

With regard to SPECT imaging, data were reconstructed using the QSPECT[19] method, based on the ordered-subsets expectation-maximization (OSEM) algorithm[20] (30 iterations, 16 subsets) with reconstruction-based compensation for attenuation, scatter, and collimator-detector response function (CDRF). The attenuation was modeled using attenuation maps derived from CT imaging. A CT image set was taken from previously acquired PET/CT data of the patient and was registered to the three SPECT images, which had been registered to each other on a HERMES (HERMES Medical Solutions; Stockholm, Sweden) workstation using a mutual information-based registration algorithm. The CT to SPECT registration included a manual fine-tuning component. Scatter compensation was performed using a fast implementation of the effective source scatter estimation method.[21] Point sources

at various distances from the face of the collimator were simulated to estimate the distance-dependent CDRF that included interactions and penetration of photons in the collimator and detector.

A calibration image of a standard vial containing a known activity of $^{111}$In (about 3 MBq) was obtained to measure the system sensitivity of both gamma-cameras.

### II.C. Calculation of absorbed dose to kidneys

Absorbed doses were derived from $^{111}$In activities in organs at different time points using three different dosimetric approaches: (1) S-value-based planar dosimetry to determine the absorbed dose to kidneys, (2) S-value-based SPECT dosimetry to determine the absorbed doses to whole kidneys, renal cortices, and medullae, and (3) SPECT-based 3D-RD to determine 3D absorbed dose distributions at the voxel level and mean absorbed doses to whole kidneys, renal cortices and medullae. Based on $^{111}$In distributions, absorbed doses were also calculated for common therapeutic radionuclides, i.e., $^{90}$Y and $^{177}$Lu, after correcting for the different physical half-lives.

#### II.C.1. S-value-based planar dosimetry

Activities derived from planar imaging at 0.5, 4, 24, and 48 h time points were fit to a monoexponential function in order to determine the time-integrated activity coefficients (TIACs). For $^{90}$Y and $^{177}$Lu, activities were adjusted at each time point due to the differing physical half-lives (64.0 h and 160 h, respectively, versus 67.3 h for $^{111}$In). Resulting TIACs for kidneys, liver, spleen, and rest of body were entered into OLINDA/EXM (version 1.1, Vanderbilt University, Nashville, TN)[22] to calculate the absorbed dose to the kidneys using S-values with adjustment for patient organ masses, as assessed through manual CT volumetry.

#### II.C.2. S-value-based SPECT dosimetry

Reconstructed SPECT data were registered to each other and VOIs were drawn for the liver, the spleen, left and right kidney cortices and medullae on the 24 h fused SPECT/CT images. VOIs were converted to masks and imported into the 3D-RD[15,16] workstation where TIACs were determined for each VOI and each radionuclide. For $^{90}$Y and $^{177}$Lu, activities were corrected for the differing physical half-life at each time point. For each radionuclide, the resulting activities were fit to a monoexponential function at both the whole-organ and voxel levels, from which the TIACs were obtained. For the whole organ, as well as for the renal cortex and medulla, the activities from the voxels within the organ at each time point were added and the total organ activities were fit to a monoexponential function. TIACs for the liver, spleen, and whole kidneys (cortex and medulla) were entered into OLINDA/EXM to calculate the absorbed dose to the whole kidneys. The TIAC for the rest of body was derived from the planar images. To calculate the absorbed dose to the renal cortex, the MIRD19 model with regional S values for the renal cortex and medulla was applied,[10] using the cortex and medulla TIACs and scaling the results to the measured masses of both compartments. Masses of both renal cortex and medulla were determined from manual segmentation of CT images. OLINDA/EXM was not used for this purpose since the implemented kidney model does not allow for mass adjustment of the cortex and the medulla. On the other hand, the absorbed dose contribution to the cortex and the medulla from the liver, the spleen, and the rest of the body was obtained with OLINDA/EXM by setting the TIAC for kidneys to zero. We assumed that the contribution from the liver, the spleen, and the rest of body to the absorbed doses to the whole kidneys, the cortex, and the medulla were equal.

#### II.C.3. SPECT-based 3D-RD

A more complete description of 3D-RD and its earlier version has been described in detail elsewhere.[15,23] Several typical procedural steps including VOI definition and activity adjustment due to half-life differences had already been implemented and described for the S-value-based SPECT dosimetry. Briefly, the next steps were as follows:

1. 10 million electrons (Auger for $^{111}$In and $^{177}$Lu, $\beta^-$ for $^{90}$Y and $^{177}$Lu) and photons (for $^{111}$In and $^{177}$Lu) were emitted and tracked using the EGSnrc Monte Carlo package. The number of histories was chosen to obtain absorbed dose rates with statistical uncertainties on the order of 10% at the voxel level and below 1% at the sub-organ level, i.e., for the renal cortex and renal medulla.
2. The energy deposition distributions from the photon and electron components obtained from the Monte Carlo simulation in Step 1 were weighted by the probability and measured activity, converted to dose rates and the values stored along with the input SPECT and CT-density data.
3. Mean absorbed doses to the whole kidneys, the cortex, and the medulla, as well as voxel absorbed doses, *D*, were calculated by fitting monoexponential functions to the dose rates calculated for the three time points as follows:

$$D = \int_0^\infty \dot{D}\, e^{-\lambda_e t}\, dt = \frac{\dot{D}_0}{\lambda_e}, \tag{1}$$

where $\dot{D}_0$ is the initial dose rate and $\lambda_e$ is the measured effective decay constant ($T_{1/2,e} = \ln(2)/\lambda_e$). In the case of some voxels with nonphysical decay constants, absorbed doses were calculated by fitting trapezoids to the data from the first three time points followed by a physical decay after the last time point.

4. The dose contribution to kidneys from the body remainder not included in the SPECT field of view, $D_{\text{kidney}\leftarrow\text{RB}}$, was added to each voxel based on the following formula:

$$\frac{D_{\text{kidney}\leftarrow\text{RB}}}{A} = \tilde{a}_{\text{RB}} \cdot S_{\text{kidney}\leftarrow\text{WB}} \cdot \frac{M_{\text{WB}} - M_{\text{SPECT}}}{M_{\text{WB}}}, \tag{2}$$

where A is the administered activity, $\tilde{a}_{RB}$ is the body remainder TIAC used in the SPECT-based approach, $M_{WB}$ is the patient's total body mass, and $M_{SPECT}$ is the mass of the patient in the SPECT field of view.

Absorbed dose to whole kidneys, renal cortices, and medullae per unit of administered activity were then compared with values obtained with OLINDA/EXM and MIRD19. Since absorbed doses were calculated at the voxel level, results were visualized in three-dimensional dose maps as well as dose volume histograms.

### II.D. Calculation of BED to kidneys using 3D-RD

For radionuclide therapy with a dose fractionated in multiple cycles, the BED takes the following form:[13]

$$\mathrm{BED} = \mathrm{D}\left(1 + \frac{\mathrm{G}(\infty)/\mathrm{N}}{\alpha/\beta}\cdot \mathrm{D}\right), \tag{3}$$

where D is the total absorbed dose given in N equal fractions, $G(\infty)$ is the generalized Lea-Catcheside factor and the $\alpha/\beta$ ratio is the repair capacity from the linear quadratic equation. This equation is valid only for a time lapse between cycles long enough to assume a complete decay of the radionuclide and full repair of sub-lethal damage. Furthermore, all biokinetic parameters are assumed constant during the overall treatment in order to retain the same factor $G(\infty)$ for each cycle. For a monoexponential decay fit to the dose rate, the $G(\infty)$-factor reduces to $\lambda_e/(\lambda_e + \mu)$ where $\mu$ is the rate of repair for sublethal damage and $\lambda_e$ is the effective decay constant for the fit to the dose rates of Eq. (1). Fits to the dose rates were monoexponential for the whole kidneys, the cortices and the medullae, as well as for most voxels. For the few voxels whose monoexponential effective decay constant was nonphysical, the general form of the $G(\infty)$-factor was solved numerically.[24] In those cases, dose rates were fit with trapezoids up until the last time point and allowed to decay physically past the last time point. For each radionuclide, the BED was calculated for the whole kidney, the cortex and the medulla using the same radiobiological parameters that were proposed by Barone *et al.*:[11] a repair half-time, $T_\mu = \ln(2)/\mu$ of 2.8 h and an $\alpha/\beta$ ratio of 2.6 Gy. Unfortunately, suborgan-specific radiobiological parameters are not available at present.

### II.E. 3D-RD-based treatment planning

Two dosimetric approaches are proposed for clinical implementation of treatment planning in PRRT: (1) *the fixed absorbed dose-based approach* where the cumulated activity that would deliver the maximum tolerated cumulated absorbed dose to the renal cortex is calculated, and (2) *the fixed BED-based approach* where the fractionation-dependent activity and the number of cycles that would deliver the maximum tolerated cumulated BED to the renal cortex is calculated.

#### II.E.1. Fixed absorbed dose-based approach

For each isotope, the administered activity, $A_D$, that would deliver a fixed absorbed dose to the cortex, $D_{cor,max}$ of 27 Gy,[11] was determined as follows:

$$\mathrm{A_D} = \frac{\mathrm{D_{cor,max}}}{\mathrm{d_{cor}}}, \tag{4}$$

where $d_{cor}$ is the mean absorbed dose to the cortex per unit of administered activity obtained from the 3D-RD calculation. Absorbed doses to the whole kidney and medulla were then scaled to the administered activities. By plotting the BED as a function of the number of cycles, N, in Eq. (3), for a fixed absorbed dose to the cortex of 27 Gy, an additional constraint may be imposed on the BED to the cortex by choosing an appropriate number of cycles.

#### II.E.2. Fixed BED-based approach

Considering a fixed BED to the cortex, Eq. (3) may be rewritten to solve for the fraction-dependent absorbed dose to the cortex, $D_{cor}(N)$. The physical solution of this equation may be expressed as follows:[13]

$$\mathrm{D_{cor}(N)} = \mathrm{N}\cdot\frac{\alpha/\beta}{2\cdot \mathrm{G}(\infty)}\left(\sqrt{1+\frac{4\cdot \mathrm{G}(\infty)\cdot \mathrm{BED_{cor}}}{\mathrm{N}\cdot\alpha/\beta}} - 1\right). \tag{5}$$

For $N\to\infty$, then $1/N\to\varepsilon$ (very small), and by using the substitution $(1+\varepsilon)^n \cong (1+n\varepsilon)$ for the radical in expression (5), the absorbed dose to the cortex for many fractions, $D_{cor}(N\to\infty)$, is equivalent to $BED_{cor}$, which is consistent with the definition of the quantity BED.

Using expression (4), the administered activity $A_{BED}(N)$ corresponding to a fixed $BED_{cor}$ value may be expressed as follows:

$$\mathrm{A_{BED}(N)} = \frac{\mathrm{D_{cor}(N)}}{\mathrm{d_{cor}}}. \tag{6}$$

Expression (6) is valid as long as the patient biodistribution and kinetics remain unchanged over the treatment duration whatever the number of cycles N. For $N\to\infty$, the asymptotic value for $A_{BED}(\infty)$ is given by

$$\mathrm{A_{BED}}(\infty) = \frac{\mathrm{BED}}{\mathrm{d_{corr}}}. \tag{7}$$

By increasing the number of cycles, N, the total administered activity to the patient can be increased while maintaining a fixed BED to the cortex. The optimal number of cycles can be determined by establishing a relevance criterion: for example, it may be considered worthwhile to increase the number of cycles as long as there is an increase of at least 5% in the total administered activity from $N-1$ cycles to N cycles.[25] The following equation formulates this idea of gain:

$$f(\mathrm{N}) = \frac{\mathrm{A_{BED}(N)} - \mathrm{A_{BED}(N-1)}}{\mathrm{A_{BED}(N)}} \tag{8}$$

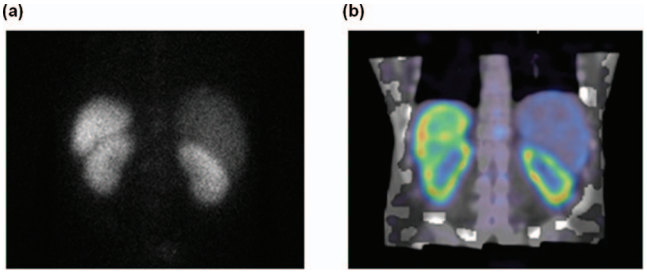


FIG. 1. Posterior planar image (a) and fused coronal SPECT/CT slice (b) of the patient 24 h post-injection of $^{111}$In-DTPA-Octreotide (185 MBq) showing high uptake in renal cortex and spleen.

and the optimal number of cycles, given a fixed BED, and a relevance criterion, $c$, is

$$N^{opt} = \max\{N | f(N) > c\}. \quad (9)$$

For the current patient case, a relevance criterion of 5% was chosen. Both maximal tolerated BED values to the cortex, $BED_{cor}$, of 28 Gy and 40 Gy were considered. The reduced-$BED_{cor}$ regimen (28 Gy) applies to patients with risk factors while the maximal $BED_{cor}$ of 40 Gy is for patients without risk factors, according to the study by Bodei *et al.*[26] The latter study was based on 12 patients with risk factors and 16 without risk factors. Both 28-Gy and 40-Gy BED thresholds were essentially derived from patients treated with $^{90}$Y-DOTATOC since only one of the five patients treated with $^{177}$Lu-DOTATATE received a cumulative BED above 28 Gy.

## III. RESULTS

Figure 1 compares planar [Fig. 1(a)] and fused SPECT/CT [Fig. 1(b)] images with $^{111}$In-DTPA-octreotide at the 24 h p.i. time point. Uptake is visible in the kidneys, the spleen, and the liver. The renal cortices and medullae can be clearly distinguished in the SPECT image, but not in the planar view.

### III.A. Calculation of absorbed dose to kidneys

The upper part of Table I compares the absorbed dose per unit activity to the whole kidneys derived from planar imaging and SPECT imaging using OLINDA/EXM, as well as the one derived from SPECT-based 3D-RD. In this single case study, the planar-based method systematically underestimates the absorbed dose compared to both SPECT-based methods, by 21% to 32%, depending on the radionuclide. Very good agreement was found between both SPECT-based methods, especially for $^{90}$Y and $^{177}$Lu. Nevertheless, a deviation of 14% was observed for $^{111}$In. Furthermore, the lower part of Table I compares the absorbed doses per unit activity to the cortex and to the medulla obtained with the MIRD19 S-values and with 3D-RD. For the cortex, deviations of −22%, +3%, and +10% were found for $^{111}$In, $^{90}$Y, and $^{177}$Lu, respectively. For the medulla, the S-values-based approach underestimated the results from 3D-RD by 41%, 1%, and 17% for $^{111}$In, $^{90}$Y and $^{177}$Lu, respectively. According to the 3D-RD calculation, the cortex-to-medulla absorbed dose ratio was 1.35 for $^{111}$In, 1.95 for $^{90}$Y, and 2.26 for $^{177}$Lu. The smaller ratio for $^{111}$In is due to the relatively homogenous energy deposition of the gamma rays within the kidneys.

### III.B. 3D-RD-based treatment planning

#### *III.B.1. Fixed absorbed dose-based approach*

Table II gives for each isotope the administered activity required to deliver an absorbed dose to the cortex, $D_{cor,max}$, of 27 Gy, using expression (4) and 3D-RD absorbed doses to the cortex per unit activity, $d_{cor}$, from Table I. Furthermore, Table II provides the main outputs of 3D-RD for the whole kidney, the cortex, and the medulla: initial dose rates, effective half-lives, $R^2$ values for the monoexponential fits to the dose rates and corresponding BED values for a single fraction (N = 1). For a given absorbed dose to cortex, the longer physical half-life of $^{177}$Lu compared to $^{111}$In and $^{90}$Y means a considerably lower initial dose rate $\dot{D}_0$ and consequently a smaller BED.

Figure 2 shows axial and coronal maps of the absorbed dose calculated with 3D-RD for $^{90}$Y. The increased absorbed dose to the cortex is not only due to the increased activity uptake with respect to the medulla (see Fig. 1), but also to the more prolonged retention of the activity within the cortex as confirmed by the effective half-lives that differ for the cortex and the medulla (see Table II). Differences are rather large for $^{90}$Y and $^{177}$Lu while they are somewhat reduced for $^{111}$In because of the higher photon dose contribution.

TABLE I. Mean absorbed doses per unit activity (in mGy/MBq) to the whole kidneys ($d_{kidney}$), the renal cortex ($d_{cor}$), and the renal medulla ($d_{med}$) calculated according to the three different dosimetric methods.

| | | Mean absorbed dose per unit activity (mGy/MBq) | | |
|---|---|---|---|---|
| Organ/tissue | Isotope | Planar and S-values | SPECT and S-values | SPECT and 3D-RD |
| Kidney (whole) | $^{111}$In | 0.15 | 0.19 | 0.22 |
| | $^{90}$Y | 1.47 | 2.00 | 1.97 |
| | $^{177}$Lu | 0.31 | 0.44 | 0.45 |
| Renal cortex | $^{111}$In | — | 0.18 | 0.23 |
| | $^{90}$Y | — | 2.26 | 2.20 |
| | $^{177}$Lu | — | 0.57 | 0.52 |
| Renal medulla | $^{111}$In | — | 0.10 | 0.17 |
| | $^{90}$Y | — | 1.12 | 1.13 |
| | $^{177}$Lu | — | 0.19 | 0.23 |

TABLE II. Administered activities (A) and absorbed doses (D) to the whole kidneys, the cortex and the medulla calculated for a fixed absorbed dose of 27 Gy to the cortex, for the different radionuclides. Most relevant outputs of 3D-RD are also indicated: initial dose rates ($\dot{D}_0$), effective half-lives ($T_{1/2,e}$), $R^2$ values showing the quality of the monoexponential fits to the dose rates, and BED values for a single fraction (N = 1).

| Isotope | A (GBq) | Organ | D (Gy) | $\dot{D}_0$ (Gy/h) | $T_{1/2,e}$ (h) | $R^2$ | BED (N = 1) (Gy) |
|---|---|---|---|---|---|---|---|
| $^{111}$In | 119.3 | Cortex | 27.0 | 0.59 | 30.2 | 0.99 | 50.7 |
| | | Medulla | 20.7 | 0.51 | 26.7 | 0.99 | 36.3 |
| | | Kidney | 25.7 | 0.57 | 29.5 | 0.99 | 47.6 |
| $^{90}$Y | 12.3 | Cortex | 27.0 | 0.61 | 30.2 | 0.99 | 50.7 |
| | | Medulla | 13.9 | 0.40 | 23.3 | 0.97 | 21.8 |
| | | Kidney | 24.2 | 0.57 | 29.1 | 0.99 | 44.0 |
| $^{177}$Lu | 52.4 | Cortex | 27.0 | 0.44 | 41.7 | 0.99 | 44.6 |
| | | Medulla | 12.1 | 0.27 | 29.5 | 0.95 | 16.8 |
| | | Kidney | 23.8 | 0.41 | 39.7 | 0.99 | 38.0 |

Figure 3 shows for each radionuclide the cumulated histograms of the time-integrated activity coefficient per voxel and the cumulated absorbed dose volume histograms (DVH) for both renal cortex [Figs. 3(a) and 3(b)] and renal medulla [Figs. 3(c) and 3(d)]. Note that the time-integrated activity is the sum of the voxel time-integrated activities, while the absorbed dose, fixed at 27 Gy in case of the renal cortex, is the average of the voxel absorbed doses. The longer physical half-life of $^{177}$Lu compared to $^{111}$In and $^{90}$Y is clearly reflected on the distribution of time-integrated activity coefficients in Figs. 3(a) and 3(c). In Figs. 3(b) and 3(d), the cumulated DVHs of $^{90}$Y and $^{177}$Lu are similar excepting the longer tail for $^{177}$Lu. This tail is due to statistical (or possibly real) fluctuations in the activity at different time points, which cause long half-lives at the voxel level. Since the physical half-life of $^{177}$Lu is much longer than that of $^{90}$Y, the dose values of these outliers were amplified. This was verified by constraining the $^{177}$Lu results to a half-life equal to the $^{90}$Y half-life and observing the disappearance of the tail (results not shown). For $^{111}$In, the absorbed dose distribution was more uniform, reflecting the dominance of long-range gamma contribution to the total absorbed dose.

To complete the fixed absorbed dose-based approach, the BED was plotted as a function of the number of cycles, N, in Fig. 4, using Eq. (3). For instance, we found that eight cycles are necessary for $^{111}$In and $^{90}$Y to keep a BED below a threshold chosen at 30 Gy while only six cycles are required for $^{177}$Lu. This difference is related to the longer delivery of the 27 Gy absorbed dose to the cortex for $^{177}$Lu, i.e., a lower initial dose rate and a longer effective half-life (see Table II).

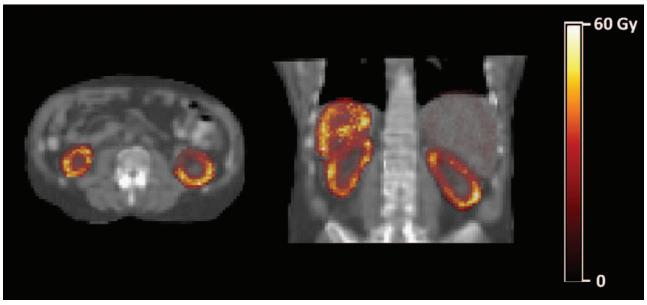


FIG. 2. Axial and coronal sections of the $^{90}$Y absorbed dose in Gy for the whole SPECT field of view shown against a CT background.

#### III.B.2. Fixed BED-based approach

The amount of activity delivering a maximal BED to the cortex, $BED_{cor}$, of 28 Gy and 40 Gy, for patients with and without risk factors, respectively,[26] was determined as a function of the number of cycles, N, using Eq. (8) in Figs. 5(a)–5(c). As the number of cycles increases, the activity that can be safely administered to the patient tends toward the asymptotic value, $A_{BED}(\infty)$. In Fig. 5(d), the gain in administered activity (and thus also in absorbed doses), is plotted as a function of the number of cycles according to Eq. (11) and a BED value of 40 Gy. The relevance criterion of 5% is indicated, from which it can be seen that the optimal number of cycles for this patient with this specific approach would be four for $^{111}$In and $^{90}$Y, and three for $^{177}$Lu. The gain in administered activity beyond this number of cycles would be smaller than 5%.

## IV. DISCUSSION

The treatment planning methodology proposed in this work enables one to perform accurate kidney dosimetry using SPECT-based 3D-RD and reduce the probability of renal toxicity in PRRT by preventing the absorbed dose or the BED to the renal cortex from exceeding the maximum tolerated value found in literature. Despite kidney protection with infusion of different regimens of positively charged amino acids,[27–30] renal function loss may become clinically evident years after PRRT.[31] Indeed, since kidney cells are slowly repairing cells, radiation damage may not manifest for several months. For this reason, accurate dosimetry is crucial to reduce renal toxicity in PRRT.

According to Table I, the planar-based method systematically underestimates the absorbed dose per unit activity to the kidneys in comparison with both SPECT-based methods. In other words, the planar-based method yields higher activity for a maximum tolerable dose to kidneys of 27 Gy. For instance, in case of $^{90}$Y, this resulting administered activity of 18.4 GBq (= 27/1.47) would deliver an absorbed dose to the cortex of 40.5 Gy and a BED of 58.3 Gy, if delivered in three cycles. Additionally, the planar method does not allow for discrimination between cortex and medulla, as they are superimposed in the images. Note that the limited resolution

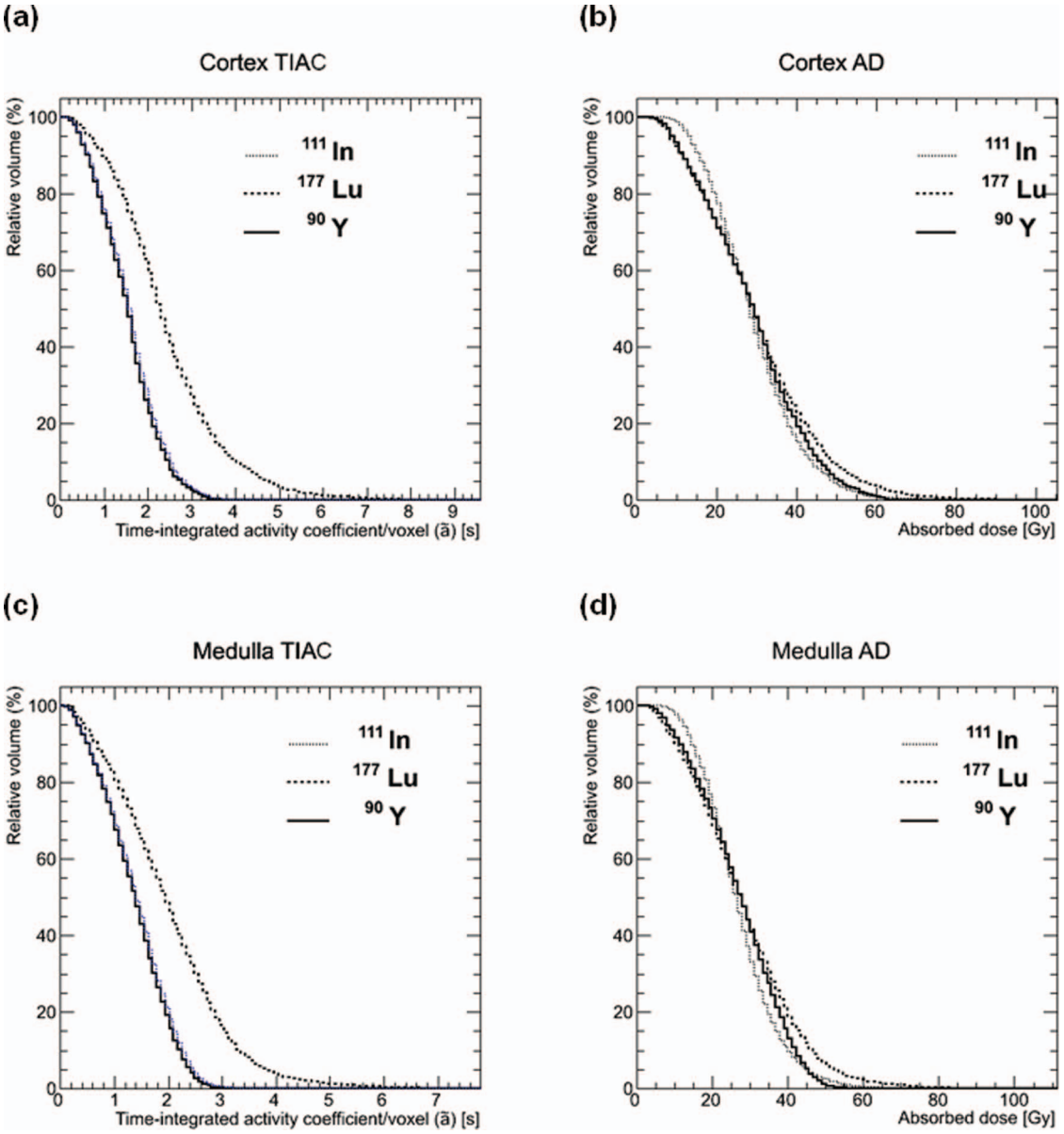


FIG. 3. Cumulated histograms of voxel time-integrated activity coefficients (TIAC) and voxel absorbed doses (AD) for the renal cortex [(a) and (b)] and the renal medulla [(c) and (d)], for all three radionuclides. Note that curves for $^{111}$In and $^{90}$Y are nearly superposed in the TIAC histograms, while the curves for $^{90}$Y and $^{177}$Lu are nearly equivalent for low values in the AD histograms.

of SPECT images allows only delineation between cortex and medulla but not the pelvic region. Considering the maximum tolerable absorbed dose to the cortex of 27 Gy, the administered activity of $^{90}$Y would be 11.9 GBq with the S-value-based SPECT dosimetry and 12.3 GBq with 3D-RD (see Table II). For $^{111}$In-DTPA-octreotide, ICRP Publication 106 reported an absorbed dose per unit activity of 0.41 mGy/MBq to the kidneys.[32] In contrast, Table I shows a value of 0.19 mGy/MBq and 0.22 mGy/MBq, depending on the SPECT-based method used. This deviation can be in part explained by the smaller mass of the ICRP reference adult male kidney (310 g for both kidneys)[33] compared to the patient's measured kidney mass (632 g). On the other hand, Cremonesi *et al.*[34] reported compatible values ranging between 0.12 and 0.91 mGy/MBq.

Regarding the 3D-RD-based treatment planning, it is informative to examine the combination of 27 Gy absorbed dose constraint with the BED constraints (28/40 Gy). Limiting the BED to 40 Gy, Fig. 4 shows that applications in two fractions are sufficient for all the radionuclides investigated. However, constraining the BED to 28 Gy would require an unreasonable number of cycles: 24 for $^{111}$In, 26 for $^{90}$Y, and 18 for $^{177}$Lu. On the other hand, the fixed BED approach provides more realistic results from a clinical perspective (Fig. 5). With the 5% relevance criterion, a patient at risk would receive a BED of 28 Gy to the cortex in three cycles of treatment corresponding to 99.2 MBq for $^{111}$In, 10.2 MBq for $^{90}$Y, and 45.6 MBq for $^{177}$Lu. A patient without risk factors would be treated with 40 Gy of BED to the cortex corresponding to four cycles of treatment with an activity of 140.0 MBq for

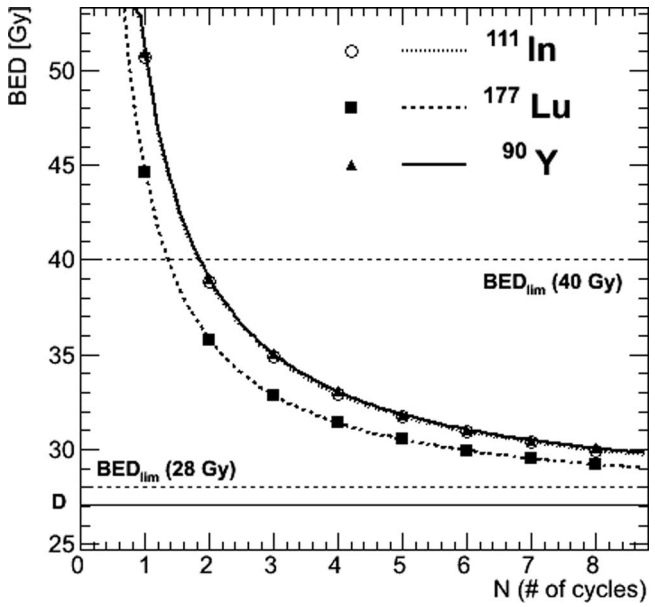


FIG. 4. Fractionation model according to the fixed absorbed dose-based approach. The BED to renal cortex varies as a function of the number of cycles, N, for a fixed absorbed dose, D, of 27 Gy to the cortex. The asymptotic limit of the BED curves is shown as a straight solid line: BED ($N \rightarrow \infty$) = D = 27 Gy). BED limits ($BED_{lim}$) of 28 and 40 Gy for patients with or without risk factors, respectively, are shown as straight dashed lines.

$^{111}$In and 14.4 MBq for $^{90}$Y, or three cycles with 61.6 MBq for $^{177}$Lu. Cumulated activities obtained for $^{111}$In and $^{90}$Y are comparable to activities administered to patients in PRRT and are somewhat higher in case of $^{177}$Lu.[14] Indeed, a typical PRRT with $^{177}$Lu-DOTATATE consists of about four cycles of about 7.4 GBq. Note that the relevance criterion of 5% is arbitrary. The treating physician might decide that for a patient without risk factor treated with $^{177}$Lu, an additional fourth cycle with a gain of 4.6% in administered activity, and thus in tumor absorbed dose, would be worthwhile, while for all radionuclides an additional fifth cycle (gain of 2.9%–3.6%) might not make sense.

While the treatment planning methodology proposed in this work focuses on limiting the absorbed dose or BED to the renal cortex, the ultimate objective is to deliver a clinically useful absorbed dose or BED to the tumor. However, the tumor absorbed dose scales with the administered activity and $\alpha/\beta$ values for tumors are rather large (5–25 Gy), resulting in only minor differences between absorbed dose and BED, unlike for the normal organs. Therefore, maximizing the total activity safely administrable seems to be a reasonable approach to potentially enhance the therapeutic outcome. Even so, when using the fixed BED approach, the gain in total administered activity, and thus tumor absorbed dose, resulting from an additional cycle must be substantial to overcome the potential effects of lower initial dose rate and longer overall treatment duration with tumor cell repopulation. Assessing the impact of fractionation is probably even more important for NETs since most of them tend to be slow-growing and relatively radio-resistant malignancies. The latter concern requires more complex modeling that has not been yet considered in our treatment planning methodology.

Not only cumulative and per-cycle absorbed dose to kidneys, but also age, hypertension, and diabetes are relevant factors affecting renal toxicity after PRRT.[26] Their variability among patients may explain the various maximum tolerated absorbed dose and BED to kidneys reported in the literature. In our treatment planning methodology, we have considered the Bodei *et al.*[26] study for two main reasons: (1) the separation between patients with and without pre-existent risk factors (mainly hypertension and diabetes) and (2) the use of the BED as the quantity of merit, with a BED threshold for renal toxicity of 28 Gy and 40 Gy for patients with and without risk factors, respectively. Thus, similarly to radioimmunotherapy where it has been proposed to customize dosing methods considering risk factors affecting hematologic toxicity,[35] the presence of risk factors affecting renal toxicity in PRRT suggest tailoring the treatment plan by selecting the suitable largest safe BED to the kidneys. In fractionated external beam radiation therapy (EBRT), it is recommended not to exceed a kidney absorbed dose $D_{5,5}$ of 23 Gy (i.e., the dose that causes severe late damage in 5% of patients within 5 years).[36] For standard EBRT with total absorbed dose delivered in 2 Gy fractions, $D_{5,5}$ translates into a $BED_{5,5}$ of 41 Gy,[13] a value very close to that used here for patients without risk factors.

Besides the kidney, the liver and bone marrow should be considered as potential dose-limiting organs in PRRT.[37,38] These considerations have not been taken into account in the present study, although adapting the methodology to a liver maximum tolerated absorbed dose or BED is rather straightforward. Since no correlation between absorbed dose to bone marrow and hematologic toxicity has yet been established in PRRT,[39,40] integration of bone marrow dosimetry into a specific treatment methodology is still out of reach.

In the present study, we used $^{111}$In-DTPA-octreotide data for planning PRRT whereas several studies demonstrated that it was not a suitable surrogate[41–43] for renal dosimetry of patients enrolled for $^{90}$Y-DOTATOC or $^{177}$Lu-DOTATATE. However, this study aimed at assessing the feasibility of the methodology and similar pharmacokinetics and biodistribution patterns within the kidneys are expected for other radiopeptides. A good treatment planning scenario would be to administer a first cycle of the radiopeptide and use the therapeutic agent for theragnostic imaging and dosimetry, and adjust for subsequent cycles. This is possible for $^{177}$Lu-peptides, but not yet realistic for $^{90}$Y-peptides since quantitative SPECT Bremsstrahlung imaging of $^{90}$Y is still challenging[44,45] and $^{86}$Y rarely accessible. Regarding pre-therapeutic dosimetry, PET imaging with $^{68}$Ga-peptides could offer interesting possibilities in terms of spatial resolution.

An important restriction in personalized image-based dosimetry is the limited spatial resolution of SPECT and PET imaging. Even though absorbed doses can be calculated at the voxel level, these cannot be trusted for single voxels and small lesions of a few voxels in size because of partial volume effects. However, when taken together as volumes of interest (VOIs), they provide additional reliable qualitative and quantitative interpretation of the VOI they form beyond the standard single average values.

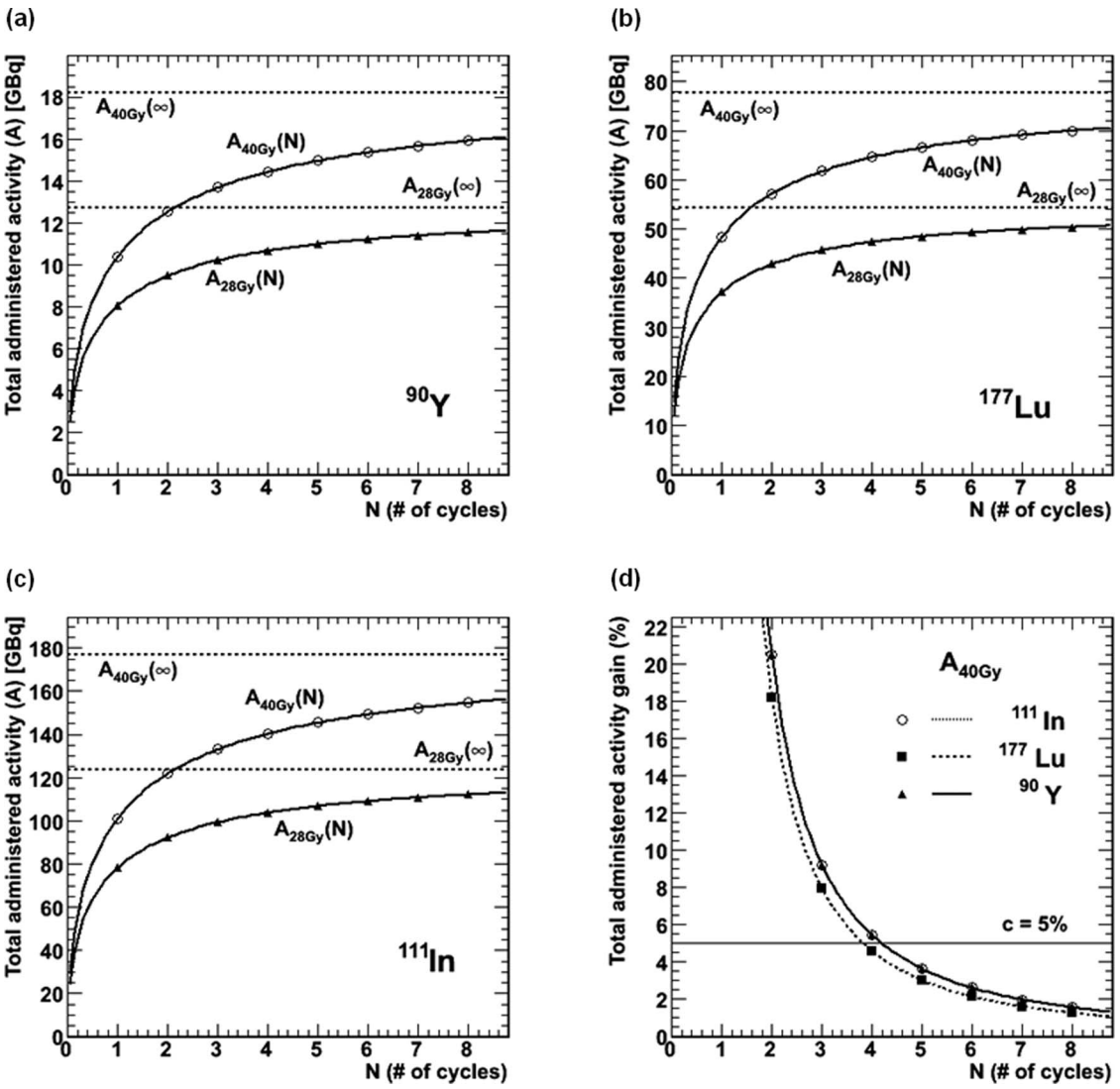


FIG. 5. Fractionation model for the fixed-BED approach. The total administered activity, $A_{BED}$, for a fixed BED, varies as a function of the number of cycles. For each isotope, $^{90}Y$ [Fig. 5(a)], $^{177}Lu$ [Fig. 5(b)], and $^{111}In$ [Fig. 5(c)], two curves are shown for a BED of 28 Gy (patients with risk factors) and for a BED of 40 Gy (patients without risk factors). Figure 5(d) shows the gain in administered activity in percentage for an increase in the number of cycles from N − 1 to N cycles for the fixed BED of 40 Gy. The relevance criterion, c, of 5% is represented by the horizontal line.

Finally, there is evidence that radiopeptides localize to smaller anatomical units than the delineation between cortex and medulla. De Jong *et al.*[46] found that activity was not distributed homogeneously but formed a striped pattern, with most of the radioactivity centered in the inner cortical zone. Clearly, better dosimetry would take into account such localization.[47] Just as clearly, patient imaging currently available such as SPECT or PET is unable to distinguish uptake at such small scales. With the greatest part of the radioactivity in the inner cortical zone, PRRT using radionuclides emitting particles with short ranges, such as Auger electron emitters and low-energy $\beta$-emitters would minimize the dose to the sensitive glomeruli in the outer renal cortex. This could explain why less renal toxicity was observed with $^{111}In$ and $^{177}Lu$ compared to $^{90}Y$.[8] Nevertheless, both radionuclides $^{177}Lu$ and $^{90}Y$ are of interest for PRRT. Indeed, the lower tissue penetration range of $^{177}Lu$ may be better suited to treat small lesions while the cross-fire effect of $^{90}Y$ may produce higher radiation burden to large and poorly vascularized tumors. Cocktails of $^{177}Lu$- and $^{90}Y$-peptides, either simultaneously or in distinct cycles, are thus appealing to treat different-sized lesions and limit renal toxicity. There is preclinical evidence that this could improve efficacy at a tolerable toxicity.[48] Although not currently implemented, the methodology developed in this work can be easily adapted to a combined $^{177}Lu/^{90}Y$ approach. In this case, since the absorbed dose from $^{177}Lu$ is delivered at lower dose rate compared to $^{90}Y$, computing the BED is essential.

## V. CONCLUSIONS

While PRRT is often administered with fixed amounts of activity per cycle, individualized dosimetry of kidneys could prevent overdosing that may cause renal toxicity and, conversely, avoid unnecessary underdosing that may reduce treatment efficacy. This work proposed a feasible clinical

approach to perform real-time, image-based, and patient-specific dosimetry in PRRT. We showed that, based on quantitative $^{111}$In-SPECT, absorbed dose and BED could be evaluated separately in the renal cortex and medulla using 3D-RD. A treatment planning methodology was developed to maximize the administered activity, including the use of optimal fractionation, while limiting the absorbed dose or the BED to the renal cortex. Based on our work, this fixed BED-based approach is the method of choice to tailor treatment protocols by providing realistic activities to administer and numbers of cycles. While fractionating the total administered activity in several therapy cycles is important to allow radiation damage repair and reduce renal toxicity, the therapeutic outcome of hyperfractionated PRRT has not yet been evaluated. In this context, the time interval between cycles may be an interesting parameter to consider and optimize to counteract tumor cell repopulation. Nonetheless, in many cases, our approach would result in higher cumulative activities to be safely administered to patients, thus potentially improving treatment efficacy thanks to the reduced ability of tumor cells to repair. As a future endpoint, the potential benefit of administering individualized "cocktails" of $^{90}$Y- and $^{177}$Lu-peptides in several cycles should be investigated using such a state-of-the-art treatment planning methodology.

## ACKNOWLEDGMENTS

The present study was partially supported by the Swiss National Science Foundation (fellowship No. PBFR2-115886), NIH/NCI Grant Nos. R01 CA116477 and R01 CA109234.

[a]Author to whom correspondence should be addressed. Electronic mail: sebastien.baechler@chuv.ch; Telephone: + 41 21 314 80 58; Fax: + 41 21 314 82 99.

[1]D. J. Kwekkeboom, J. Mueller-Brand, G. Paganelli, L. B. Anthony, S. Pauwels, L. K. Kvols, T. M. O'Dorisio, R. Valkema, L. Bodei, M. Chinol, H. R. Maecke, and E. P. Krenning, "Overview of results of peptide receptor radionuclide therapy with 3 radiolabeled somatostatin analogs," J. Nucl. Med. **46**(Suppl. 1), 62S–66S (2005).

[2]R. Valkema, M. De Jong, W. H. Bakker, W. A. Breeman, P. P. Kooij, P. J. Lugtenburg, F. H. De Jong, A. Christiansen, B. L. Kam, W. W. De Herder, M. Stridsberg, J. Lindemans, G. Ensing, and E. P. Krenning, "Phase I study of peptide receptor radionuclide therapy with [In-DTPA]octreotide: The Rotterdam experience," Semin. Nucl. Med. **32**, 110–122 (2002).

[3]J. C. Reubi, H. R. Macke, and E. P. Krenning, "Candidates for peptide receptor radiotherapy today and in the future," J. Nucl. Med. **46**(Suppl. 1), 67S–75S (2005).

[4]D. J. Kwekkeboom, B. L. Kam, M. van Essen, J. J. Teunissen, C. H. van Eijck, R. Valkema, M. de Jong, W. W. de Herder, and E. P. Krenning, "Somatostatin-receptor-based imaging and therapy of gastroenteropancreatic neuroendocrine tumors," Endocr. Relat. Cancer **17**, R53–R73 (2010).

[5]J. P. Esser, E. P. Krenning, J. J. Teunissen, P. P. Kooij, A. L. van Gameren, W. H. Bakker, and D. J. Kwekkeboom, "Comparison of [(177)Lu-DOTA(0),Tyr(3)]octreotate and [(177)Lu-DOTA(0),Tyr(3)]octreotide: Which peptide is preferable for PRRT?," Eur. J. Nucl. Med. Mol. Imaging **33**, 1346–1351 (2006).

[6]B. Lambert, M. Cybulla, S. M. Weiner, C. Van De Wiele, H. Ham, R. A. Dierckx, and A. Otte, "Renal toxicity after radionuclide therapy," Radiat. Res. **161**, 607–611 (2004).

[7]M. van Essen, E. P. Krenning, B. L. Kam, M. de Jong, R. Valkema, and D. J. Kwekkeboom, "Peptide-receptor radionuclide therapy for endocrine tumors," Nat. Rev. Endocrinol. **5**, 382–393 (2009).

[8]M. Cremonesi, F. Botta, A. Di Dia, M. Ferrari, L. Bodei, C. De Cicco, A. Rossi, M. Bartolomei, R. Mei, S. Severi, M. Salvatori, G. Pedroli, and G. Paganelli, "Dosimetry for treatment with radiolabelled somatostatin analogues: A review," Q. J. Nucl. Med. Mol. Imaging **54**, 37–51 (2010).

[9]W. S. Snyder, M. R. Ford, G. G. Warner, and S. B. Watson, *''S,'' Absorbed Dose per Unit Cumulated Activity for Selected Radionuclides and Organs: MIRD Pamphlet No. 11* (Society of Nuclear Medicine, New York, 1975).

[10]L. G. Bouchet, W. E. Bolch, H. P. Blanco, B. W. Wessels, J. A. Siegel, D. A. Rajon, I. Clairand, and G. Sgouros, "MIRD Pamphlet No. 19: Absorbed fractions and radionuclide S values for six age-dependent multiregion models of the kidney," J. Nucl. Med. **44**, 1113–1147 (2003).

[11]R. Barone, F. Borson-Chazot, R. Valkema, S. Walrand, F. Chauvin, L. Gogou, L. K. Kvols, E. P. Krenning, F. Jamar, and S. Pauwels, "Patient-specific dosimetry in predicting renal toxicity with (90)Y-DOTATOC: Relevance of kidney volume and dose rate in finding a dose-effect relationship," J. Nucl. Med. **46**(Suppl. 1), 99S–106S (2005).

[12]R. G. Dale, "The application of the linear-quadratic dose-effect equation to fractionated and protracted radiotherapy," Br. J. Radiol. **58**, 515–528 (1985).

[13]S. Baechler, R. F. Hobbs, A. R. Prideaux, R. L. Wahl, and G. Sgouros, "Extension of the biological effective dose to the MIRD schema and possible implications in radionuclide therapy dosimetry," Med. Phys. **35**, 1123–1134 (2008).

[14]B. W. Wessels, M. W. Konijnenberg, R. G. Dale, H. B. Breitz, M. Cremonesi, R. F. Meredith, A. J. Green, L. G. Bouchet, A. B. Brill, W. E. Bolch, G. Sgouros, and S. R. Thomas, "MIRD Pamphlet No. 20: The effect of model assumptions on kidney dosimetry and response–implications for radionuclide therapy," J. Nucl. Med. **49**, 1884–1899 (2008).

[15]A. R. Prideaux, H. Song, R. F. Hobbs, B. He, E. C. Frey, P. W. Ladenson, R. L. Wahl, and G. Sgouros, "Three-dimensional radiobiologic dosimetry: Application of radiobiologic modeling to patient-specific 3-dimensional imaging-based internal dosimetry," J. Nucl. Med. **48**, 1008–1016 (2007).

[16]R. F. Hobbs, R. L. Wahl, M. A. Lodge, M. S. Javadi, S. Y. Cho, D. T. Chien, M. E. Ewertz, C. E. Esaias, P. W. Ladenson, and G. Sgouros, "124I PET-based 3D-RD dosimetry for a pediatric thyroid cancer patient: Real-time treatment planning and methodologic comparison," J. Nucl. Med. **50**, 1844–1847 (2009).

[17]J. A. Siegel, S. R. Thomas, J. B. Stubbs, M. G. Stabin, M. T. Hays, K. F. Koral, J. S. Robertson, R. W. Howell, B. W. Wessels, D. R. Fisher, D. A. Weber, and A. B. Brill, "MIRD Pamphlet No. 16: Techniques for quantitative radiopharmaceutical biodistribution data acquisition and analysis for use in human radiation dose estimates," J. Nucl. Med. **40**, 37S–61S (1999).

[18]S. Baechler, R. F. Hobbs, A. R. Prideaux, M. Recordon, A. Bischof-Delaloye, and G. Sgouros, "Estimates of radiation-absorbed dose to kidneys in patients treated with 90Y-ibritumomab tiuxetan," Cancer Biother. Radiopharm. **23**, 633–639 (2008).

[19]B. He, Y. Du, X. Y. Song, W. P. Segars, and E. C. Frey, "A Monte Carlo and physical phantom evaluation of quantitative In-111SPECT," Phys. Med. Biol. **50**, 4169–4185 (2005).

[20]H. M. Hudson and R. S. Larkin, "Accelerated image-reconstruction using ordered subsets of projection data," IEEE Trans. Med. Imaging **13**, 601–609 (1994).

[21]D. J. Kadrmas, E. C. Frey, S. S. Karimi, and B. M. Tsui, "Fast implementations of reconstruction-based scatter compensation in fully 3D SPECT image reconstruction," Phys. Med. Biol. **43**, 857–873 (1998).

[22]M. G. Stabin, R. B. Sparks, and E. Crowe, "OLINDA/EXM: The second-generation personal computer software for internal dose assessment in nuclear medicine," J. Nucl. Med. **46**, 1023–1027 (2005).

[23]G. Sgouros and K. S. Kolbert, "The three-dimensional internal dosimetry software package, 3D-ID," in *Therapeutic Applications of Monte Carlo Calculations in Nuclear Medicine*, edited by H. Zaidi and G. Sgouros (Institute of Physics, Philadelphia, PA, 2002), pp. 249–261.

[24]R. F. Hobbs and G. Sgouros, "Calculation of the biological effective dose (BED) for piece-wise defined dose-rate fits.," Med. Phys. **36**, 904–907 (2009).

[25]A. R. Stahl, L. Freudenberg, A. Bockisch, and W. Jentzen, "A novel view on dosimetry-related radionuclide therapy: Presentation of a calculatory model and its implementation for radioiodine therapy of metastasized differentiated thyroid carcinoma," Eur. J. Nucl. Med. Mol. Imaging **36**, 1147–1155 (2009).

[26]L. Bodei, M. Cremonesi, M. Ferrari, M. Pacifici, C. M. Grana, M. Bartolomei, S. M. Baio, M. Sansovini, and G. Paganelli, "Long-term evaluation of renal toxicity after peptide receptor radionuclide therapy with 90Y-

DOTATOC and 177Lu-DOTATATE: The role of associated risk factors," Eur. J. Nucl. Med. Mol. Imaging **35**, 1847–1856 (2008).
[27]E. J. Rolleman, R. Valkema, M. de Jong, P. P. Kooij, and E. P. Krenning, "Safe and effective inhibition of renal uptake of radiolabelled octreotide by a combination of lysine and arginine," Eur. J. Nucl. Med. Mol. Imaging **30**, 9–15 (2003).
[28]M. de Jong and E. Krenning, "New advances in peptide receptor radionuclide therapy," J. Nucl. Med. **43**, 617–620 (2002).
[29]F. Jamar, R. Barone, I. Mathieu, S. Walrand, D. Labar, P. Carlier, J. de Camps, H. Schran, T. Chen, M. C. Smith, H. Bouterfa, R. Valkema, E. P. Krenning, L. K. Kvols, and S. Pauwels, "86Y-DOTA0)-D-Phe1-Tyr3-octreotide (SMT487)–a phase 1 clinical study: Pharmacokinetics, biodistribution and renal protective effect of different regimens of amino acid co-infusion," Eur. J. Nucl. Med. Mol. Imaging **30**, 510–518 (2003).
[30]L. Bodei, M. Cremonesi, S. Zoboli, C. Grana, M. Bartolomei, P. Rocca, M. Caracciolo, H. R. Macke, M. Chinol, and G. Paganelli, "Receptor-mediated radionuclide therapy with 90Y-DOTATOC in association with amino acid infusion: A phase I study," Eur. J. Nucl. Med. Mol. Imaging **30**, 207–216 (2003).
[31]R. Valkema, S. A. Pauwels, L. K. Kvols, D. J. Kwekkeboom, F. Jamar, M. de Jong, R. Barone, S. Walrand, P. P. Kooij, W. H. Bakker, J. Lasher, and E. P. Krenning, "Long-term follow-up of renal function after peptide receptor radiation therapy with (90)Y-DOTA(0),Tyr(3)-octreotide and (177)Lu-DOTA(0), Tyr(3)-octreotate," J. Nucl. Med. **46**(Suppl. 1), 83S–91S (2005).
[32]ICRP, *Radiation Dose to Patients from Pharmaceuticals* (Pergammon, 2009).
[33]ICRP, *Basic Anatomical and Physiological Data for Use in Radiological Protection: Reference Values* (Pergammon, 2003).
[34]M. Cremonesi, M. Ferrari, L. Bodei, G. Tosi, and G. Paganelli, "Dosimetry in Peptide radionuclide receptor therapy: A review," J. Nucl. Med. **47**, 1467–1475 (2006).
[35]S. Baechler, R. F. Hobbs, H. A. Jacene, F. O. Bochud, R. L. Wahl, and G. Sgouros, "Predicting hematologic toxicity in patients undergoing radioimmunotherapy with 90Y-ibritumomab tiuxetan or 131I-tositumomab," J. Nucl. Med. **51**, 1878–1884 (2010).
[36]B. Emami, J. Lyman, A. Brown, L. Coia, M. Goitein, J. E. Munzenrider, B. Shank, L. J. Solin, and M. Wesson, "Tolerance of normal tissue to therapeutic irradiation," Int. J. Radiat. Oncol., Biol. Phys. **21**, 109–122 (1991).
[37]L. Bodei, M. Cremonesi, C. Grana, P. Rocca, M. Bartolomei, M. Chinol, and G. Paganelli, "Receptor radionuclide therapy with 90Y-[DOTA]0-Tyr3-octreotide (90Y-DOTATOC) in neuroendocrine tumours," Eur. J. Nucl. Med. Mol. Imaging **31**, 1038–1046 (2004).
[38]D. Bushnell, T. O'Dorisio, Y. Menda, T. Carlisle, P. Zehr, M. Connolly, M. Karwal, S. Miller, S. Parker, and H. Bouterfa, "Evaluating the clinical effectiveness of 90Y-SMT 487 in patients with neuroendocrine tumors," J. Nucl. Med. **44**, 1556–1560 (2003).
[39]R. Barone, S. Walrand, M. Konijnenberg, R. Valkema, L. K. Kvols, E. P. Krenning, S. Pauwels, and F. Jamar, "Therapy using labelled somatostatin analogues: Comparison of the absorbed doses with 111In-DTPA-D-Phe1-octreotide and yttrium-labelled DOTA-D-Phe1-Tyr3-octreotide," Nucl. Med. Commun. **29**, 283–290 (2008).
[40]F. Forrer, E. P. Krenning, P. P. Kooij, B. F. Bernard, M. Konijnenberg, W. H. Bakker, J. J. Teunissen, M. de Jong, K. van Lom, W. W. de Herder, and D. J. Kwekkeboom, "Bone marrow dosimetry in peptide receptor radionuclide therapy with [177Lu-DOTA(0),Tyr(3)]octreotate," Eur. J. Nucl. Med. Mol. Imaging **36**, 1138–1146 (2009).
[41]S. Pauwels, R. Barone, S. Walrand, F. Borson-Chazot, R. Valkema, L. K. Kvols, E. P. Krenning, and F. Jamar, "Practical dosimetry of peptide receptor radionuclide therapy with (90)Y-labeled somatostatin analogs," J. Nucl. Med. **46**(Suppl. 1), 92S–98S (2005).
[42]G. J. Forster, M. J. Engelbach, J. J. Brockmann, H. J. Reber, H. G. Buchholz, H. R. Macke, F. R. Rosch, H. R. Herzog, and P. R. Bartenstein, "Preliminary data on biodistribution and dosimetry for therapy planning of somatostatin receptor positive tumours: Comparison of (86)Y-DOTATOC and (111)In-DTPA-octreotide," Eur. J. Nucl. Med. **28**, 1743–1750 (2001).
[43]A. Helisch, G. J. Forster, H. Reber, H. G. Buchholz, R. Arnold, B. Goke, M. M. Weber, B. Wiedenmann, S. Pauwels, U. Haus, H. Bouterfa, and P. Bartenstein, "Pre-therapeutic dosimetry and biodistribution of 86Y-DOTA-Phe1-Tyr3-octreotide versus 111In-pentetreotide in patients with advanced neuroendocrine tumours," Eur. J. Nucl. Med. Mol. Imaging **31**, 1386–1392 (2004).
[44]D. Minarik, K. Sjogreen-Gleisner, O. Linden, K. Wingardh, J. Tennvall, S. E. Strand, and M. Ljungberg, "90Y Bremsstrahlung imaging for absorbed-dose assessment in high-dose radioimmunotherapy," J. Nucl. Med. **51**, 1974–1978 (2010).
[45]X. Rong, Y. Du, M. Ljungberg, E. Rault, S. Vandenberghe, and E. C. Frey, "Development and evaluation of an improved quantitative 90Y bremsstrahlung SPECT method," Med. Phys. **39**, 2346–2358 (2012).
[46]M. De Jong, R. Valkema, A. Van Gameren, H. Van Boven, A. Bex, E. P. Van De Weyer, J. D. Burggraaf, M. Korner, J. C. Reubi and E. P. Krenning, "Inhomogeneous localization of radioactivity in the human kidney after injection of [(111)In-DTPA]octreotide," J. Nucl. Med. **45**, 1168–1171 (2004).
[47]M. Konijnenberg, M. Melis, R. Valkema, E. Krenning, and J. M. de, "Radiation dose distribution in human kidneys by octreotides in peptide receptor radionuclide therapy Assessment of hepatic toxicity from treatment with 90Y-SMT 487 (OctreoTher(TM)) in patients with diffuse somatostatin receptor positive liver metastases," J. Nucl. Med. **48**, 134–142 (2007).
[48]M. de Jong, W. A. Breeman, R. Valkema, B. F. Bernard, and E. P. Krenning, "Combination radionuclide therapy using 177Lu- and 90Y-labeled somatostatin analogs," J. Nucl. Med. **46**(Suppl. 1), 13S–17S (2005).